JOURNAL OF COMPUTATIONAL PHYSICS 9, 440–465 (1972)

Use of Fast Fourier Transforms for Solving Partial Differential Equations in Physics

ROLAND C. LE BAIL

CERN, Geneva, Switzerland

Received March 12, 1971

The use of fast Fourier techniques for the direct solution of an important class of elliptic, parabolic, and hyperbolic partial differential equations in two dimensions is described. Extensions to higher-order and higher-dimension equations as well as to integrodifferential equations are presented, and several numerical examples with their resulting precision and timing are reported.

1. INTRODUCTION

The numerical solution of partial differential equations arising from physics is one of the most important tasks for high-speed digital computers. At present, most existing codes are restricted to particular differential equations, and there is none which applies to a broad range of problems. Recently, the fast Fourier transform (FFT), which has been known for a few years, was successfully applied to the direct solution of the Laplace operator in two and three dimensions [1–4]. The object of the present report is the extension of FFT techniques to the solution of a broad class of linear second-order partial differential equations, including evolutive equations such as the vibrating string equation and the diffusion equation. Because of their importance in mathematical physics, we will consider the subclass of linear second-order two-dimensional partial differential equations (LSOTDPDE) of the form

$$\frac{\partial^2\phi(x, y)}{\partial x^2} + a(y)\frac{\partial^2\phi(x, y)}{\partial y^2} + b(y)\frac{\partial\phi(x, y)}{\partial y} + c(y)\,\phi(x, y) = \rho(x, y). \qquad (1)$$

This subclass includes the following equations in physics:

(i) elliptic equations such as Laplace and Poisson equations in planar geometry

$$\frac{\partial^2\phi}{\partial x^2} + \frac{\partial^2\phi}{\partial y^2} = \rho(x, y) \qquad (2)$$

in cylindrical geometry

$$\frac{\partial^2\phi}{\partial z^2} + \frac{\partial^2\phi}{\partial r^2} + \frac{1}{r}\frac{\partial\phi}{\partial r} = \rho(z, r) \qquad \text{in} \quad (r, z), \tag{3}$$

$$\frac{\partial^2\phi}{\partial\theta^2} + r^2\frac{\partial^2\phi}{\partial r^2} + r\frac{\partial\phi}{\partial r} = r^2\rho(r, \theta) \qquad \text{in} \quad (r, \theta) \tag{4}$$

with Dirichlet, Neumann, or periodic boundary conditions on a closed contour;

(ii) parabolic equations such as the heat conduction or diffusion equation

$$\frac{\partial^2\phi}{\partial x^2} = a^2\frac{\partial\phi}{\partial t} + b(x, t) \tag{5}$$

with Cauchy conditions;

(iii) hyperbolic equations such as the vibrating-string equation

$$\frac{\partial^2\phi}{\partial x^2} - \frac{1}{c^2}\frac{\partial^2\phi}{\partial t^2} = 0 \tag{6}$$

with Cauchy conditions;

(iv) Helmholtz-type equations

$$\frac{\partial^2\phi}{\partial x^2} + \frac{\partial^2\phi}{\partial y^2} + k^2\phi = 0 \tag{7}$$

with k known and the usual boundary conditions.

In the remainder of this paper the various Fourier transforms associated with the corresponding boundary conditions for the x direction will be covered without great detail, assuming that the reader is familar with Hockney's paper [1]. Along the second direction, which can be either spatial or temporal, the associated method of solution will be derived. Finally, generalizations to higher-dimension, higher-order equations, integrodifferential equations as well as equations containing a first-derivative term with respect to x will be outlined.

2. Finite Difference Formulation

The number of mesh points along the x direction will be either $M - 1$, M, or $M + 1$ depending on the type of boundary conditions for that direction. In the

following it is assumed that M is restricted to discrete values of the form $M = 2^Q$, where Q is a positive integer, allowing the use of FFT techniques.

The absence of a first-derivative term with respect to x in Eq. (1) leads to the following symmetric nine-point finite difference formula [5]:

$$\sum_{k=-1}^{1} \{\alpha_k(J)[\phi(I-1, J+k) + \phi(I+1, J+k)] + \beta_k(J)\,\phi(I, J+k)\} = \rho(I, J) \quad (8)$$

for all interior mesh points (I, J) of Fig. 1.

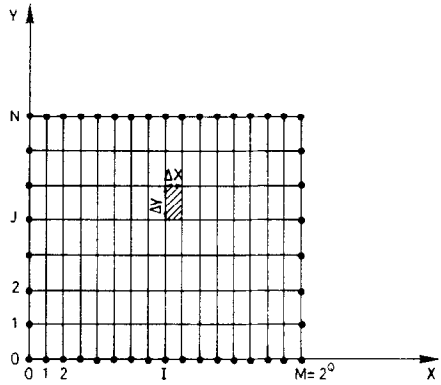

FIG. 1. Finite difference mesh. The above illustration corresponds to the solution of an elliptic equation. The unknown function ϕ has prescribed values at the solid-circular points all around the boundary of the rectangular domain, while the values of the source term ρ are given for every interior point. The solution of Eq. (8) allows the evaluation of ϕ for every interior point of the domain.

In the case of a parabolic equation characterized by $a(y) \equiv 0$, the above finite difference equation is replaced by a six-point formula,

$$\sum_{k=-1}^{0} \{\alpha_k(J)[\phi(I-1, J+k) + \phi(I+1, J+k)] + \beta_k(J)\,\phi(I, J+k)\} = \rho(I, J). \quad (9)$$

From now on, the consideration of coefficients $\alpha_k(J)$ and $\beta_k(J)$, which depend explicitly on J for Eqs. (8) and (9) and which allow the solution of, for example, Eqs. (3) and (4), will be dropped without any loss of generality in the application of the method but with much benefit to the clarity (see the remark at the end of Section 4).

When the α_k's and β_k's are independent of J, that is when Eq. (1) has constant

coefficients a, b, c, one can derive explicit expressions for Eqs. (8) and (9). Equation (8) leads to the following five-point stencil:

	$a\alpha^2 + \frac{b}{2}\alpha\Delta X$	
1	$-2(1 + a\alpha^2) + c(\Delta X)^2$	1
	$a\alpha^2 - \frac{b}{2}\alpha\Delta X$	

$$\phi(*, *) = (\Delta X)^2 \rho(I, J), \tag{10}$$

where $\alpha = \Delta X/\Delta Y$ and $(*, *)$ stands for $(I - 1, J)$, (I, J), $(I + 1, J)$, $(I, J - 1)$, and $(I, J + 1)$.

For $b \neq 0$, stencil equation (10) is exact up to the third order in x and up to the second order in y in the neighborhood of a point.

For $b = 0$, it is exact up to the third order in both directions.

When $a = 1$, $b = c = 0$, and $\Delta Y = \Delta X$, stencil equation (10) reduces to the familiar finite difference form of Poisson's equation

	1	
1	−4	1
	1	

$$\phi(*, *) = (\Delta X)^2 \rho(I, J). \tag{11}$$

Equation (9), which corresponds to $a = 0$, leads to the following six-point stencil:

1	$-2 + 2b\alpha\Delta X + c(\Delta X)^2$	1
1	$-2 - 2b\alpha\Delta X + c(\Delta X)^2$	1

$$\phi(*, *) = \begin{array}{|c|}\hline 1 \\ \hline 1 \\ \hline \end{array} \; (\Delta X)^2 \rho(*, *). \tag{12}$$

For $b \neq 0$, stencil equation (12) is exact up to the third order in x and up to the second order in y in the neighborhood of a point.

For $b = 0$, it is exact up to the third order in x and to any order in y. When $b = -1$, $c = 0$, and $\Delta Y = \Delta X = 1$, stencil equation (12) reduces to

1	−4	1
1	0	1

$\phi(*, *) =$

1
1

$\rho(*, *).$ (13)

For the following derivation, it is convenient to simplify further the writing of stencil equations (10) and (12) by setting

$$\begin{aligned} \Gamma(I, J) &= (\Delta X)^2 \rho(I, J), \\ SS &= a\alpha^2 - (b/2)\,\alpha\,\Delta X, \\ SC &= 2(1 + a\alpha^2) - c(\Delta X)^2, \\ SN &= a\alpha^2 + (b/2)\,\alpha\,\Delta X, \\ SL &= -2 - 2b\alpha\,\Delta X + c(\Delta X)^2, \\ SU &= -2 + 2b\alpha\,\Delta X + c(\Delta X)^2. \end{aligned} \tag{14}$$

Stencil equations (10) and (12) take, respectively, the simple forms

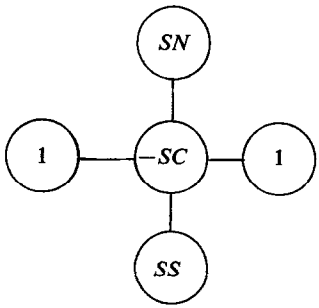

$\phi(*, *) = \Gamma(I, J)$ (15)

and

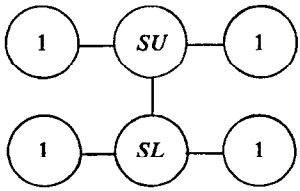

$\phi(*, *) =$

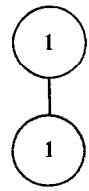

$\Gamma(*, *).$ (16)

3. Boundary Conditions for the x Direction and Associated Fourier Transforms

For the three types of equations—that is: elliptic, parabolic, and hyperbolic equations—the x axis is always a spatial direction subject to boundary conditions at both ends. In this section we will consider four types of useful boundary conditions for the x direction.

(a) *The function ϕ has given values at each end of the x-range.* Explicitly, one has for row J of Fig. 1.

$$\begin{aligned} \phi(0, J) &= \phi_L(J), \\ \phi(M, J) &= \phi_R(J). \end{aligned} \tag{17}$$

When $I = 1$ or $I = M - 1$, the stencil equations (15) and (16) collect, so to speak, boundary conditions (17) and, since they are known quantities, one transfers them to the right-hand side of stencil equations (15) and (16) by redefining

$$\begin{aligned} \Gamma(1, J) &:= \Gamma(1, J) - \phi_L(J), \\ \Gamma(M - 1, J) &:= \Gamma(M - 1, J) - \phi_R(J). \end{aligned} \tag{18}$$

One can therefore assume that the end conditions are $\phi = 0$, and the appropriate Fourier transform is a sine analysis and synthesis.

Letting U stand for either Γ or ϕ, one has

Analysis

$$U_S(J) = \frac{2}{M} \sum_{I=1}^{M-1} U(I, J) \sin\left(\frac{\pi SI}{M}\right) \qquad (1 \leqslant S \leqslant M - 1); \tag{19}$$

Synthesis

$$U(I, J) = \sum_{S=1}^{M-1} U_S(J) \sin\left(\frac{\pi IS}{M}\right) \qquad (1 \leqslant I \leqslant M - 1). \tag{20}$$

(b) *The function ϕ has given derivatives at each end of the x range.* In this case, the finite difference mesh of Fig. 1 has to be extended by column $I = -1$ on the left-hand side and column $I = M + 1$ on the right-hand side. For row J, using a central difference formula for the partial derivative with respect to x, one has

$$\begin{aligned} \phi(1, J) - \phi(-1, J) &= 2\,\Delta X\, D_L(J), \\ \phi(M + 1, J) - \phi(M - 1, J) &= 2\,\Delta X\, D_R(J). \end{aligned} \tag{21}$$

Again, for $I = 0$ and $I = M$, stencil equations (15) and (16) collect the boundary conditions (21) and, after redefining,

$$\begin{aligned} \Gamma(0, J) &:= \Gamma(0, J) + 2\,\Delta X\, D_L(J), \\ \Gamma(M, J) &:= \Gamma(M, J) - 2\,\Delta X\, D_R(J). \end{aligned} \tag{22}$$

One can assume the end conditions to be $\partial\phi/\partial x = 0$, and the appropriate Fourier transform is a cosine analysis and synthesis:

Analysis

$$U_S(J) = \frac{2}{M} \sum_{I=0}^{M} E(I, M)\, U(I, J) \cos\left(\frac{\pi SI}{M}\right) \qquad (0 \leqslant S \leqslant M); \tag{23}$$

Synthesis

$$U(I, J) = \sum_{S=0}^{M} E(S, M)\, U_S(J) \cos\left(\frac{\pi IS}{M}\right) \qquad (0 \leqslant I \leqslant M), \tag{24}$$

where

$$E(i, j) = \begin{cases} \frac{1}{2} & \text{if } i = 0 \text{ or } i = j \\ 1, & \text{otherwise.} \end{cases}$$

(c) *The function is periodic along the x direction.* In this case column $I = M$, which is identical to column $I = 0$, can be suppressed, and one has the following Fourier transform:

Analysis

$$\begin{aligned} U_S(J) &= \frac{2}{M} \sum_{I=0}^{M-1} F(S, M/2)\, U(I, J) \cos\left(\frac{2\pi SI}{M}\right) \qquad (0 \leqslant S \leqslant M/2), \\ U_S(J) &= \frac{2}{M} \sum_{I=0}^{M-1} U(I, J) \sin\left(\frac{2\pi[S - (M/2)]\, I}{M}\right) \qquad \left(\frac{M}{2} + 1 \leqslant S \leqslant M - 1\right); \end{aligned} \tag{25}$$

Synthesis

$$\begin{aligned} U(I, J) = &\sum_{S=0}^{M/2} F(S, M/2)\, U_S(J) \cos\left(\frac{2\pi IS}{M}\right) \\ &+ \sum_{S=(M/2)+1}^{M-1} U_S(J) \sin\left(\frac{2\pi I[S - (M/2)]}{M}\right) \qquad (0 \leqslant I \leqslant M - 1), \end{aligned} \tag{26}$$

where

$$F(i, j) = \begin{cases} 1/\sqrt{2} & \text{if } i = 0 \text{ or } i = j \\ 1, & \text{otherwise.} \end{cases}$$

(d) *The function ϕ has given values on the left end and derivatives on the right end of the x range.* These mixed types of boundary conditions are very useful when one is confronted with a symmetric problem, in which case one studies the left half and sets $\partial\phi/\partial x = 0$ for the right-end boundary condition.

In this case, the finite difference mesh of Fig. 1 needs to be completed by column $I = M + 1$, and one has in finite difference form

$$\begin{aligned} \phi(0, j) &= \phi_L(J), \\ \phi(M+1, J) - \phi(M-1, J) &= 2\,\Delta X\, D_R(J). \end{aligned} \tag{27}$$

Again, for $I = 1$ and $I = M$, stencil equations (15) and (16) collect the boundary conditions (27) and, after redefining,

$$\begin{aligned} \Gamma(1, J) &:= \Gamma(1, J) - \phi_L(J), \\ \Gamma(M, J) &:= \Gamma(M, J) - 2\,\Delta X\, D_R(J). \end{aligned} \tag{28}$$

One can assume that $\phi = 0$ on the left-hand side and $\partial\phi/\partial x = 0$ on the right-hand side of the x range and the appropriate Fourier transform is as follows:

Analysis

$$\begin{aligned} U_S(J) &= \frac{4}{M} \sum_{I=1}^{M/2} U(2I-1, J) \sin\left(\frac{\pi S(2I-1)}{2M}\right), \\ U_{S+1}(J) &= \frac{4}{M} \sum_{I=1}^{M/2-1} U(2I, J) \sin\left(\frac{\pi SI}{M}\right) + \frac{2}{M} U(M, J) \sin\left(\frac{\pi S}{2}\right) \\ &\qquad (S = 1, 3, 5, \ldots, M-1); \end{aligned} \tag{29}$$

Synthesis

$$\begin{aligned} U(I, J) &= \sum_{S=1}^{M/2} U_{2S-1}(J) \sin\left(\frac{\pi I(2S-1)}{2M}\right) \qquad (I = 1, 3, 5, \ldots, M-1), \\ U(I, J) &= \sum_{S=1}^{M/2} U_{2S}(J) \sin\left(\frac{\pi I(2S-1)}{2M}\right) \qquad (I = 2, 4, 6, \ldots, M). \end{aligned} \tag{30}$$

4. Reduction of the Two-Dimensional Problem to a Set of One-Dimensional Problems along the Second Dimension Using the Above Fourier Transforms

The above four types of transforms are used to reduce the two-dimensional stencil equations (15) and (16) to one-dimensional ones.

We first illustrate the technique for boundary conditions 3(a), and then state the results corresponding to the other three boundary conditions.

Let us start with stencil equation (15), which we rewrite in more conventional form

$$\phi(I-1, J) - SC\phi(I, J) + \phi(I+1, J) + SS\phi(I, J-1) + SN\phi(I, J+1) = \Gamma(I, J). \tag{31}$$

Replacing U by ϕ and Γ in system (20), we get

$$\phi(I, J) = \sum_{S=1}^{M-1} \phi_S(J) \sin\left(\frac{\pi IS}{M}\right) \qquad (1 \leqslant I \leqslant M-1), \tag{32}$$

$$\Gamma(I, J) = \sum_{S=1}^{M-1} \Gamma_S(J) \sin\left(\frac{\pi IS}{M}\right) \qquad (1 \leqslant I \leqslant M-1). \tag{33}$$

Replacing the above values of ϕ and Γ into Eq. (31) and making use of the following identity:

$$\sin\left(\frac{\pi(I-1)S}{M}\right) + \sin\left(\frac{\pi(I+1)S}{M}\right) = 2\cos\left(\frac{\pi S}{M}\right)\sin\left(\frac{\pi IS}{M}\right), \tag{34}$$

one gets after some rearranging

$$\sum_{S=1}^{M-1} \left\{SS\phi_S(J-1) + \left[2\cos\left(\frac{\pi S}{M}\right) - SC\right]\phi_S(J) + SN\phi_S(J+1)\right\} \sin\left(\frac{\pi IS}{M}\right)$$
$$= \sum_{S=1}^{M-1} \Gamma_S(J) \sin\left(\frac{\pi IS}{M}\right) \tag{35}$$

which is equivalent to the following system:

$$SS\phi_S(J-1) + \left[2\cos\left(\frac{\pi S}{M}\right) - SC\right]\phi_S(J) + SN\phi_S(J+1) = \Gamma_S(J)$$
$$(1 \leqslant S \leqslant M-1). \tag{36}$$

Using the same technique, stencil equation (16) reduces to

$$\left[2\cos\left(\frac{\pi S}{M}\right) + SL\right]\phi_S(J-1) + \left[2\cos\left(\frac{\pi S}{M}\right) + SU\right]\phi_S(J)$$
$$= \Gamma_S(J-1) + \Gamma_S(J) \qquad (1 \leqslant S \leqslant M-1). \tag{37}$$

For a given value of S, Eqs. (36) and (37) are finite difference "molecules" representative of a one-dimensional problem along the second dimension.

Equation (36) is a three-point recurrence formula involving rows $J-1$, J, and $J+1$, while Eq. (37) is a two-point recurrence formula involving rows $J-1$ and J. Both one-dimensional problems can be solved using the appropriate boundary conditions: for $J=0$ and $J=N$ in the elliptic case and simply $J=0$ in the parabolic and hyperbolic cases.

Fortunately, boundary conditions of types 3(b) and 3(c) lead to the same equations (36) and (37), the only change being the ranges of S values, which are $0 \leqslant S \leqslant M$ and $0 \leqslant S \leqslant M-1$, respectively.

Boundary conditions of the mixed type 3(d) require a special treatment; in this case, Eq. (36) is replaced by

$$\begin{aligned} &SS\phi_{2S}(J-1) + 2\cos\left(\frac{\pi(2S-1)}{2M}\right)\phi_{2S-1}(J) - SC\phi_{2S}(J) + SN\phi_{2S}(J+1) \\ &\quad = \Gamma_{2S}(J), \\ &SS\phi_{2S-1}(J-1) + 2\cos\left(\frac{\pi(2S-1)}{2M}\right)\phi_{2S}(J) - SC\phi_{2S-1}(J) + SN\phi_{2S-1}(J+1) \\ &\quad = \Gamma_{2S-1}(J) \qquad (S=1, 2,\ldots, M/2). \end{aligned} \tag{38}$$

With U standing for both ϕ and Γ, we define new functions according to

$$\begin{aligned} U^{+}_{2S}(J) &= U_{2S-1}(J) + U_{2S}(J), \\ U^{-}_{2S}(J) &= U_{2S-1}(J) - U_{2S}(J). \end{aligned} \tag{39}$$

Finally, combining equations of system (38), we get

$$\begin{aligned} &SS\phi^{+}_{2S}(J-1) + \left[2\cos\left(\frac{\pi(2S-1)}{2M}\right) - SC\right]\phi^{+}_{2S}(J) + SN\phi^{+}_{2S}(J+1) = \Gamma^{+}_{2S}(J), \\ &SS\phi^{-}_{2S}(J-1) - \left[2\cos\left(\frac{\pi(2S-1)}{2M}\right) + SC\right]\phi^{-}_{2S}(J) + SN\phi^{-}_{2S}(J+1) = \Gamma^{-}_{2S}(J) \\ &\qquad\qquad (S=1, 2,\ldots, M/2). \end{aligned} \tag{40}$$

Following the same path, stencil equation (16) would reduce to

$$\begin{aligned} &\left[2\cos\left(\frac{\pi(2S-1)}{2M}\right) + SL\right]\phi^{+}_{2S}(J-1) + \left[2\cos\left(\frac{\pi(2S-1)}{2M}\right) + SU\right]\phi^{+}_{2S}(J) \\ &\quad = \Gamma^{+}_{2S}(J-1) + \Gamma^{+}_{2S}(J), \\ &\left[2\cos\left(\frac{\pi(2S-1)}{2M}\right) - SL\right]\phi^{-}_{2S}(J-1) + \left[2\cos\left(\frac{\pi(2S-1)}{2M}\right) - SU\right]\phi^{-}_{2S}(J) \\ &\quad = -(\Gamma^{-}_{2S}(J-1) + \Gamma^{-}_{2S}(J)) \qquad (S=1, 2,\ldots, M/2). \end{aligned} \tag{41}$$

Equations (40) and (41) are essentially of the same form as Eqs. (36) and (37), and can therefore be solved using the same technique.

Remark. We can now see that the restriction placed on constant coefficients for Eq. (1) could be lifted without harm to the method; in the case of variable coefficients with respect to the y-coordinate or variable mesh size ΔY, one would simply have coefficients depending on J for recurrence formulas (36), (37) and (40), (41), and the one-dimensional problems could still be solved with the appropriate boundary conditions.

5. Types of Equations and Associated Methods of Solution Along the Second Dimension

The solution of Eqs. (36), (37) or (40), (41) depends essentially on the type of equation one has to solve. This section will therefore be divided into three parts covering the elliptic, parabolic, and hyperbolic cases, respectively.

5.1. *Elliptic Equations* ($a > 0$)

In this case, one has top and bottom boundary conditions for the vertical y direction of the form

$$\begin{aligned} &\text{Bottom:} && \alpha_B\phi + \beta_B(\partial\phi/\partial y) = g_1(x), \\ &\text{Top:} && \alpha_T\phi + \beta_T(\partial\phi/\partial y) = g_2(x); \end{aligned} \tag{42}$$

or in finite difference form,

$$\begin{aligned} \alpha_B\phi(I, 0) + \beta_B[\phi(I, 1) - \phi(I, -1)]/2\,\Delta Y &= g_1(I), \\ \alpha_T\phi(I, N) + \beta_T[\phi(I, N+1) - \phi(I, N-1)]/2\,\Delta Y &= g_2(I), \end{aligned} \tag{43}$$

where in the case of boundary conditions of type 3(a), I runs from 1 to $M - 1$.

Now let us summarize the whole solution of an elliptic problem having the above type of boundary conditions for the x direction and boundary conditions (43) for the y direction.

(i) Using Eqs. (18), one redefines $\Gamma(1, J)$ and $\Gamma(M-1, J)$ for J running from 0 to N.

(ii) Using FFT for system (19), one gets

$$\Gamma_S(J) = \frac{2}{M}\sum_{I=1}^{M-1}\Gamma(I, J)\sin\left(\frac{\pi SI}{M}\right) \qquad (1 \leqslant S \leqslant M-1), \tag{44}$$

J running from 0 to N, and,

$$g_{1_S} = \frac{2}{M} \sum_{I=1}^{M-1} g_1(I) \sin\left(\frac{\pi SI}{M}\right)$$
$$g_{2_S} = \frac{2}{M} \sum_{I=1}^{M-1} g_2(I) \sin\left(\frac{\pi SI}{M}\right) \qquad (1 \leqslant S \leqslant M-1). \tag{45}$$

(iii) For each S-value $(1 \leqslant S \leqslant M-1)$, one uses the classical Gauss elimination method to solve the three-point recurrence system of Eqs. (36),

$$SS\phi_S(J-1) + \left[2\cos\left(\frac{\pi S}{M}\right) - SC\right]\phi_S(J) + SN\phi_S(J+1) = \Gamma_S(J) \qquad (0 \leqslant J \leqslant N) \tag{46}$$

subject to boundary conditions

$$\alpha_B\phi_S(0) + \beta_B[\phi_S(1) - \phi_S(-1)]/2\,\Delta Y = g_{1_S}\,,$$
$$\alpha_T\phi_S(N) + \beta_T[\phi_S(N+1) - \phi_S(N-1)]/2\,\Delta Y = g_{2_S}\,. \tag{47}$$

Note. Figure 1 corresponds to given values of function ϕ on the top and bottom of the mesh; that is, $\alpha_B = 1$, $\beta_B = 0$, $\alpha_T = 1$, $\beta_T = 0$.

(iv) Again, using FFT for system (20), one finally gets the solution

$$\phi(I, J) = \sum_{S=1}^{M-1} \phi_S(J) \sin\left(\frac{\pi IS}{M}\right) \qquad (1 \leqslant I \leqslant M-1), \tag{48}$$

J running from 0 to N.

The Gauss elimination method used to solve system (46) subject to boundary conditions (47) is an error-reducing scheme and is therefore always stable.

5.2. *Parabolic Equations* ($a = 0$)

In this case the problem is of the evolutive type; the vertical axis being usually the time direction, there are only initial conditions at the bottom of the mesh of the form

$$\alpha_B\phi + \beta_B(\partial\phi/\partial t) = g_1(x), \tag{49}$$

or in finite-difference form

$$\alpha_B\phi(I, 0) + \beta_B[\phi(I, 0) - \phi(I, -1)]/\Delta Y = g_1(I). \tag{50}$$

Again for boundary conditions of type 3(a) for the x direction, steps (i), (ii), (iv) above are essentially the same, but step (iii) is completely different. Instead of Eq. (36), one has the two-point recurrence formula (37),

$$\left[2\cos\left(\frac{\pi S}{M}\right) + SL\right]\phi_S(J-1) + \left[2\cos\left(\frac{\pi S}{M}\right) + SU\right]\phi_S(J) = \Gamma_S(J-1) + \Gamma_S(J) \qquad (1 \leqslant J \leqslant N) \tag{51}$$

subject to the initial condition

$$\alpha_B\phi_S(0) + \beta_B[\phi_S(0) - \phi_S(-1)]/\Delta Y = g_{1_S}. \tag{52}$$

For example, in the case of given values along the bottom boundary, one has $\alpha_B = 1$ and $\beta_B = 0$. One then gets $\phi_S(0) = g_{1_S}$ from Eq. (52) and, using a step-by-step method, one "marches" using Eq. (51) for $J = 1, 2, \ldots, N$ and computes successively $\phi_S(1)$, $\phi_S(2), \ldots, \phi_S(N)$.

In contrast with the implicit scheme used for the elliptic case, the above step-by-step method is numerically stable if

$$\left|2\cos\left(\frac{\pi S}{M}\right) + SU\right| > \left|2\cos\left(\frac{\pi S}{M}\right) + SL\right| \qquad \text{for all } S \quad (1 \leqslant S \leqslant M-1); \tag{53}$$

or, using Eqs. (14) and setting $\epsilon^2(S) = 2\,[1 - \cos(\pi S/M)]$,

$$|-\epsilon^2(S) + 2b\alpha\,\Delta X + c(\Delta X)^2| > |-\epsilon^2(S) - 2b\alpha\,\Delta X + c(\Delta X)^2| \qquad \text{for all } S \quad (1 \leqslant S \leqslant M-1). \tag{54}$$

Rather than study condition (54) in detail, we can outline an interesting result for the case of the "well-posed" problem (corresponding to a physically positive diffusion) of the heat equation (5) for which $b = -a^2$, $c = 0$. For this case Eq. (54) becomes

$$\epsilon^2(S) + 2a^2\alpha\,\Delta X > |-\epsilon^2(S) + 2a^2\alpha\,\Delta X| \tag{55}$$

and we readily see that whatever the positive value of α is, inequality (55) is always satisfied, which means that there is no restriction placed on the value of

$$a^2\alpha\,\Delta X = a^2[(\Delta X)^2/\Delta Y],$$

while for other methods one requires

$$(1/a^2)[\Delta Y/(\Delta X)^2] < (1/2). \tag{56}$$

In addition to the unrestricted value ΔY, the present method allows the use of a higher-precision six-point formula, while the other step-by-step methods are restricted to a lower-precision four-point "forward" stencil.

5.3. *Hyperbolic Case* ($a < 0$)

We are again confronted with a problem of the evolutive type; the vertical axis is generally the time direction, the initial conditions being of the form

$$\begin{aligned} \phi &= g_1(x) \\ \text{and} \qquad \partial\phi/\partial t &= g_2(x), \end{aligned} \tag{57}$$

or in finite-difference form

$$\begin{aligned} \phi(I, 0) &= g_2(I), \\ \phi(I, 1) - \phi(I, 0) &= \Delta Y g_2(I). \end{aligned} \tag{58}$$

Again, for boundary conditions of type 3(a) for the x-direction, step (iii) has to be treated somewhat differently.

In this case, one uses the system of equations (36),

$$SS\phi_S(J-1) + \left[2\cos\left(\frac{\pi S}{M}\right) - SC\right]\phi_S(J) + SN\phi_S(J+1) = \Gamma_S(J) \qquad (0 \leqslant J \leqslant N) \tag{59}$$

subject to the following initial conditions:

$$\begin{aligned} \phi_S(0) &= g_{1S}\,, \\ \phi_S(1) - \phi_S(0) &= \Delta Y g_{2S}\,. \end{aligned} \tag{60}$$

One first computes $\phi_S(0)$ and $\phi_S(1)$ using system (60); then using the three-point recurrence formula (59) for $J = 1, 2, \ldots, N-1$, one successively gets $\phi_S(2)$, $\phi_S(3), \ldots, \phi_S(N)$. For this case we must again perform a stability analysis.

The corresponding amplification matrix is

$$G = \begin{pmatrix} \dfrac{SC - 2\cos(\pi S/M)}{SN} & -\dfrac{SS}{SN} \\ 1 & 0 \end{pmatrix} \qquad \text{for all } S \qquad (1 \leqslant S \leqslant M-1). \tag{61}$$

Rather than perform a detailed stability analysis, let us consider the case of the vibrating-string equation (6) for which formula (61) becomes

$$G = \begin{pmatrix} 2\left[1 - \dfrac{c^2}{\alpha^2}\epsilon^2(S)\right] & -1 \\ 1 & 0 \end{pmatrix} \qquad (1 \leqslant S \leqslant M-1), \tag{62}$$

where $\epsilon^2(S) = 1 - \cos(\pi S/M)$.

The two eigenvalues are given by

$$\lambda^2 - 2[1 - (c^2/\alpha^2)\,\epsilon^2(S)]\,\lambda + 1 = 0 \qquad (1 \leqslant S \leqslant M-1). \tag{63}$$

If $(c^2/\alpha^2)\,\epsilon^2(S) \leqslant 2$, both roots have absolute value 1 and, since $\epsilon^2_{\max}(S) \simeq 2$, we have the following stability condition:

$$(c^2/\alpha^2) < 1 \qquad \text{or} \qquad c^2(\Delta Y/\Delta X)^2 < 1. \tag{64}$$

Again, the present method allows the use of a higher-precision nine-point formula, while the other step-by-step methods are restricted to a lower-precision five-point "forward" stencil.

6. Existing Programs and Examples

A general program has been developed which solves Eq. (1) with constant coefficients on a rectangular mesh. The program is simply fed with the coefficients of the LSOTDPDE, the source term, and the appropriate boundary conditions. The variety of boundary conditions according to the type of equation is best summarized by the tableau of Fig. 2.

Another more general program for which the coefficients of the LSOTDPDE are functions of the second dimension has been developed; it accomodates the same variety of boundary conditions as the first one, but accepts general stencil equations (8) or (9).

We are now going to give three example pertaining to the three types of equations and their resulting timing.

6.1. *Elliptic Equation* ($a > 0$)

This example, which is taken from electrostatics, is concerned with the solution of Poisson's equation in two-dimensional planar geometry

$$(\partial^2\phi/\partial x^2) + (\partial^2\phi/\partial y^2) = -\rho. \tag{65}$$

After normalization, one has the following boundary conditions and source term illustrated by Fig. 3a:

$$\begin{aligned} &\phi(-1, y) = 1 \quad \text{and} \quad \phi(1, y) = 0 \quad \text{for} \quad 0 \leqslant y \leqslant 1, \\ &\frac{\partial\phi(x, 0)}{\partial y} = 0 \quad \text{and} \quad \phi(x, 1) = \tfrac{1}{2}(1 - x) \quad \text{for} \quad -1 \leqslant x \leqslant 1. \end{aligned} \tag{66}$$

ρ is zero everywhere except at the origin where its value is normalized to 1.

The condition $\partial\phi(x, 0)/\partial y = 0$ implies symmetry with respect to the x axis.

Figure 3b displays the resulting potential map. The mesh has 64 divisions along x and 40 along y; the corresponding timing is 0.477 sec on the CERN CDC 6600

computer with a relative precision [with respect to the adopted five-point stencil (15)] of 10^{-11}.

Partial differential equation:

$$\frac{\partial^2\phi(x,y)}{\partial x^2} + a\frac{\partial^2\phi(x,y)}{\partial y^2} + b\frac{\partial\phi(x,y)}{\partial y} + c\phi(x,y) = \rho(x,y),$$

where ϕ is the unknown function while ρ is the known source term.

The coefficients a, b, and c as well as the cell ratio $\Delta X/\Delta Y$ and the mesh size ($M = 2^Q$ along X and N along Y) are given parameters.

Boundary conditions for X:

1) $\phi(0,y) = f_1(y), \phi(M,y) = f_2(y)$

2) $\dfrac{\partial\phi(0,y)}{\partial x} = f_3(y), \dfrac{\partial\phi(M,y)}{\partial x} = f_4(y)$

3) Periodic along x

4) $\phi(0,y) = f_5(y), \dfrac{\partial\phi(M,y)}{\partial x} = f_6(y)$

Boundary conditions for Y (or t):

1) *Elliptic case* ($a > 0$)

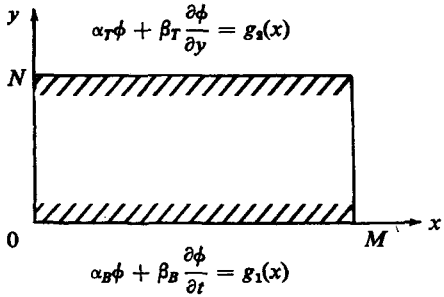

2) *Parabolic case* ($a = 0$):

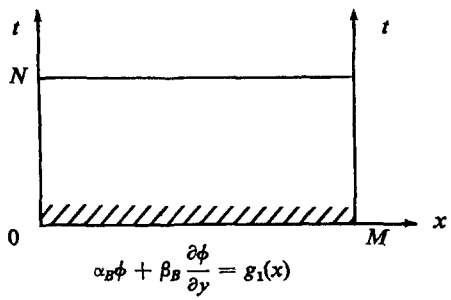

3) *Hyperbolic case* ($a < 0$)

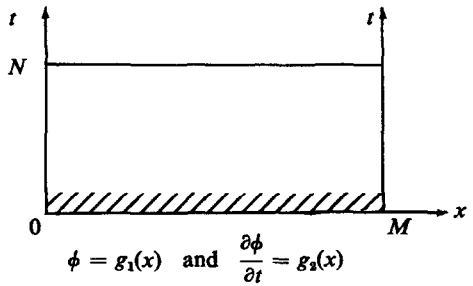

FIGURE 2

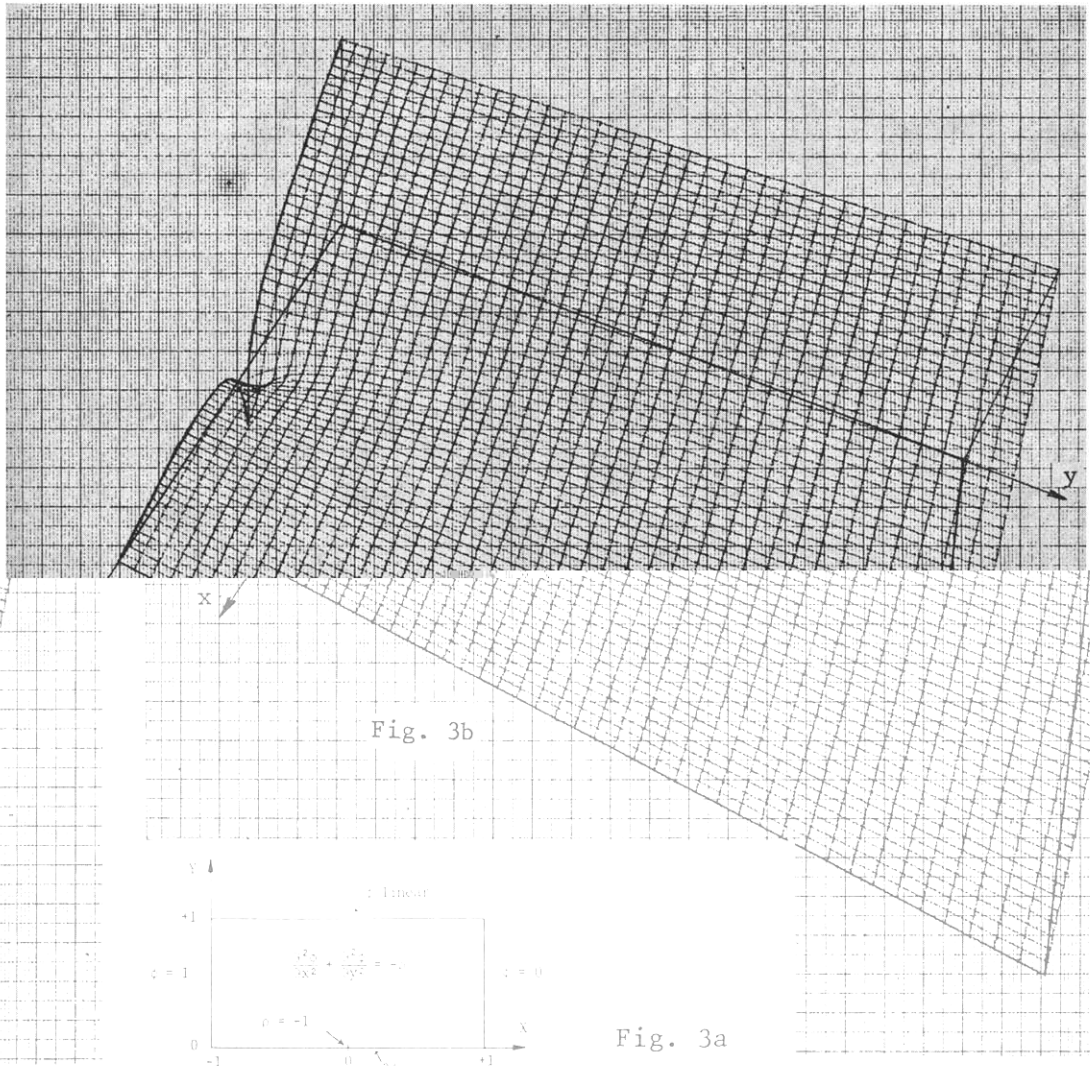

FIGURE 3

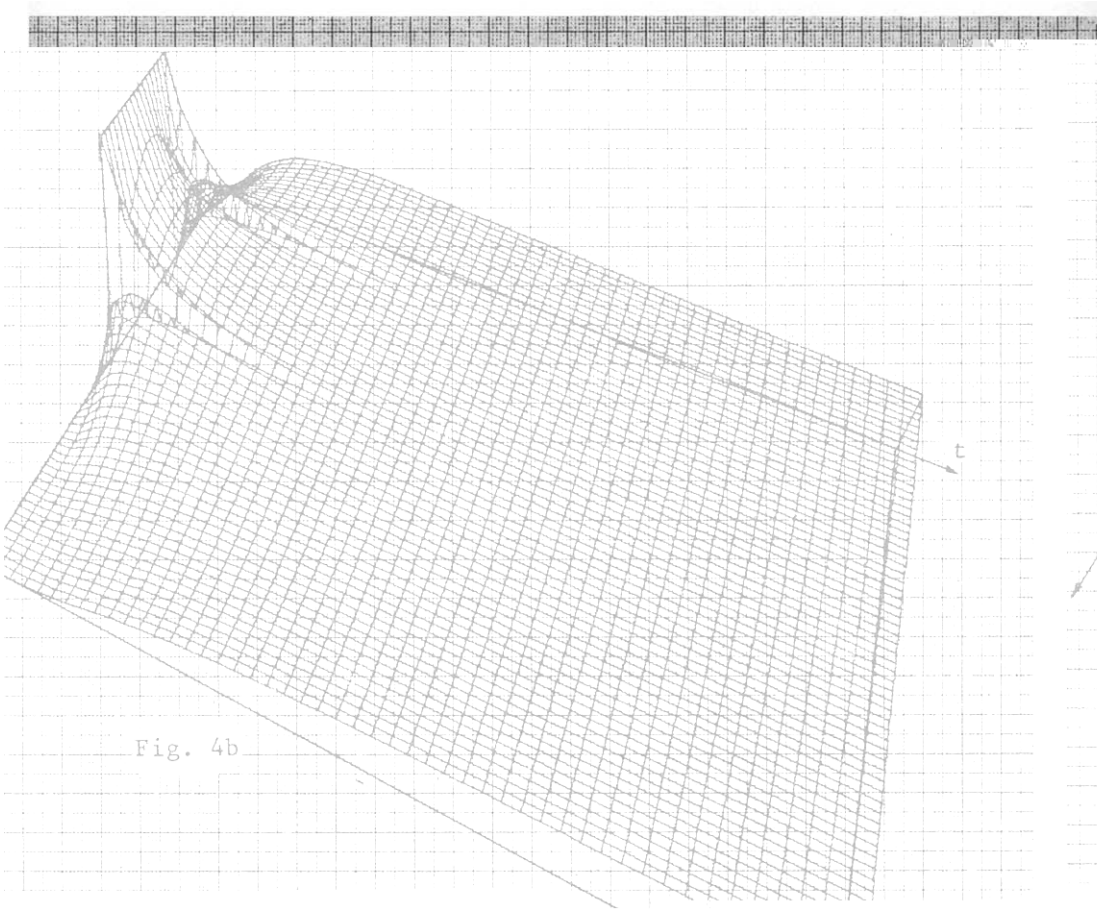

Fig. 4b

6.2. *Parabolic Equation* ($a = 0$)

A typical problem associated with a parabolic equation may be illustrated by the following equation:

$$(\partial^2 T/\partial x^2) - (1/\alpha^2)(\partial T/\partial t) = \beta, \tag{67}$$

where T can be interpreted as the temperature at time t of an element of a thin rod at a distance x from the center.

In this case we choose $1/\alpha^2 = 0.1$ and $\beta = 0$ for the numerical solution, and after normalization, one has the following initial and boundary conditions illustrated by Fig. 4a:

$$\begin{aligned} T(x, 0) &= 0 \quad \text{for} \quad -1 \leqslant x \leqslant -\tfrac{1}{2} \quad \text{or} \quad 0 \leqslant x \leqslant 1, \\ T(x, 0) &= 1 \quad \text{for} \quad -\tfrac{1}{2} \leqslant x \leqslant 0, \\ \frac{\partial T(-1, t)}{\partial x} &= 0 \quad \text{and} \quad \frac{\partial T(1, t)}{\partial x} = 0 \quad \text{for} \quad t \geqslant 0. \end{aligned} \tag{68}$$

The last two equations (68) imply that the heat flow at each end of the rod is null; therefore, as t increases, the initial temperature plateau of constant height 1 and width $\frac{1}{4}$ of the x range will diffuse in such a way that for large enough t the whole x range will be at the final temperature $T = \frac{1}{4}$.

Figure 4b displays the resulting evolutive phenomenon and one can see clearly that for large t the temperature T tends to one quarter of the initial height of the plateau. The mesh used has 64 divisions along x and 100 along y, the corresponding timing is 1.088 sec on the CERN CDC 6600 computer with a relative precision [with respect to the adopted six-point stencil (16)] of 10^{-11}.

6.3. *Hyperbolic Equation* ($a < 0$)

This example which is borrowed from Lanczos [6] is associated with the differential equation of the vibrating string:

$$(\partial^2 v/\partial x^2) - (\partial^2 v/\partial t^2) = 0, \tag{69}$$

where v is the displacement of the string at a given point x and a given time t.

After normalization, let us have the following initial and boundary conditions illustrated by Fig. 5a:

$$\begin{aligned} v(x, 0) &= 1 + x \quad \text{for} \quad -1 \leqslant x \leqslant 0, \\ v(-1, t) &= 0 \quad \text{and} \quad \frac{\partial v(0, t)}{\partial x} = 0 \quad \text{for} \quad t \geqslant 0. \end{aligned} \tag{70}$$

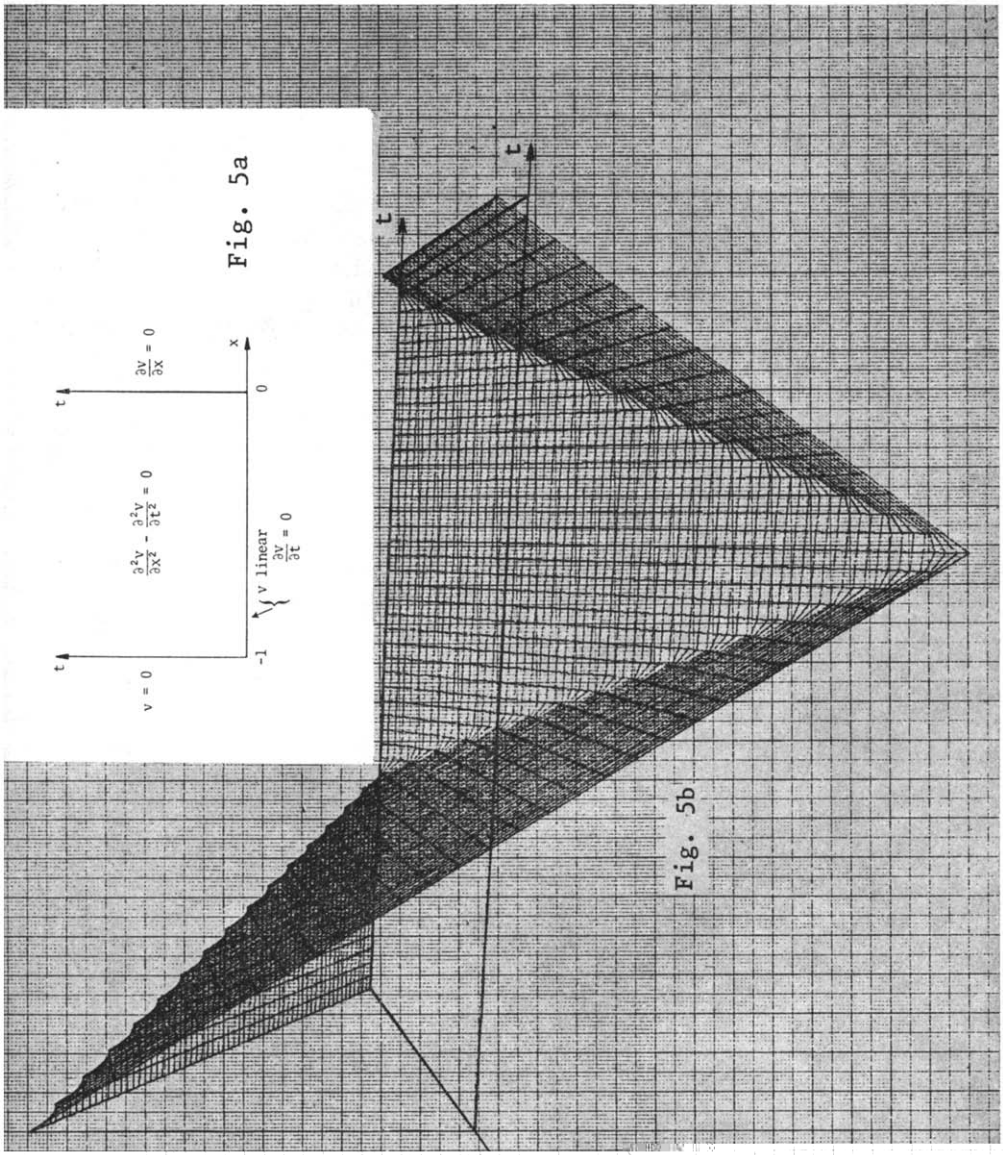
Fig. 5a
t
x
v = 0
-1
0
$\frac{\partial^2 v}{\partial x^2} - \frac{\partial^2 v}{\partial t^2} = 0$
v linear
$\frac{\partial v}{\partial t} = 0$
$\frac{\partial v}{\partial x} = 0$
Fig. 5b
t
t
t

FIGURE 5

The initial condition means that the string is excited by "plucking" it at $x = 0$, while the boundary conditions imply that the string is symmetric with respect to $x = 0$; so we have only considered the left half.

Figure 5b displays the resulting evolutive phenomenon. The rather strange behavior of the string is as follows: the outer contour remains at rest while a straight line moves down with uniform speed, truncating the triangle to a quadrangle of diminishing height until the figure collapses. The same phenomenon repeats itself downward in reverse sequence until the reverse image of the triangle is restored, and then the center of the string moves back up again. The mesh used has 64 divisions along x and 200 along y, the corresponding timing is 9.012 sec on the CERN CDC 6600 computer with a relative precision [with respect to the adopted five-point stencil (15)] of 10^{-11}.

7. Extensions and Concluding Remarks

7.1. *Extension of the Method to Higher-Order Equations*

Equation (1) can be solved successively, allowing for the solution of higher-order equations. For example, the following fourth-order equation:

$$\frac{\partial^4\phi}{\partial x^4} + (a_1 + a_2)\frac{\partial^4\phi}{\partial x^2\,\partial y^2} + a_1a_2\frac{\partial^4\phi}{\partial y^4} + (b_1 + b_2)\frac{\partial^3\phi}{\partial x^2\,\partial y} + (a_1b_2 + b_1a_2)\frac{\partial^3\phi}{\partial y^3} + (c_1 + c_2)\frac{\partial^2\phi}{\partial x^2} + (a_1c_2 + b_1b_2 + c_1a)\frac{\partial^2\phi}{\partial y^2} + (b_1c_2 + c_1b_2)\frac{\partial\phi}{\partial y} + c_1c_2\phi = \rho \tag{71}$$

with boundary conditions

$$\frac{\partial^2\phi}{\partial x^2} + a_2\frac{\partial^2\phi}{\partial y^2} + b_2\frac{\partial\phi}{\partial y} + c_2\phi, \qquad \text{and } \phi \text{ given on a rectangular contour } (C),$$

can be factorized and solved in two steps using an intermediate function ψ according to

$$\begin{aligned} &\text{(i)} \quad \frac{\partial^2\psi}{\partial x^2} + a_1\frac{\partial^2\psi}{\partial y^2} + b_1\frac{\partial\psi}{\partial y} + c_1\psi = \rho \qquad \text{with } \psi \text{ given on } (C) \\ &\text{(ii)} \quad \frac{\partial^2\phi}{\partial x^2} + a_2\frac{\partial^2\phi}{\partial y^2} + b_2\frac{\partial\phi}{\partial y} + c_2\phi = \psi \qquad \text{with } \phi \text{ given on } (C). \end{aligned} \tag{72}$$

A well-known example of the above factorization is the biharmonic equation for which one has: $a_1 = a_2 = 1$, $b_1 = b_2 = c_1 = c_2 = 0$,

$$\frac{\partial^4 \phi}{\partial x^4} + 2\frac{\partial^4 \phi}{\partial x^2 \partial y^2} + \frac{\partial^4 \phi}{\partial y^2} = \rho$$

with (73)

$$\frac{\partial^2 \phi}{\partial x^2} + \frac{\partial^2 \phi}{\partial y^2} = 0, \qquad \text{and} \qquad \phi = 0 \text{ on } (C),$$

in which case one takes the intermediate function ψ and successively solves

$$\begin{aligned} &\frac{\partial^2 \psi}{\partial x^2} + \frac{\partial^2 \psi}{\partial y^2} = \rho \qquad \text{with} \quad \psi = 0 \text{ on } (C), \\ &\frac{\partial^2 \phi}{\partial x^2} + \frac{\partial^2 \phi}{\partial y^2} = \psi \qquad \text{with} \quad \phi = 0 \text{ on } (C), \end{aligned} \tag{74}$$

allowing for the use of a simpler stencil equation than the one required for the direct solution of Eq. (73).

7.2. *Extension of the Method to Higher-Dimension Equations*

The method can be extended to three- and four-dimensional problems as in the case of the relativity theory.

For the three-dimensional case, the partial differential equation must be of the form

$$\frac{\partial^2 \phi}{\partial x^2} + a(z)\frac{\partial^2 \phi}{\partial y^2} + b(z)\frac{\partial^2 \phi}{\partial z^2} + c(z)\frac{\partial \phi}{\partial z} + d(z)\,\phi = \rho, \tag{75}$$

where z can either be a true dimension or the time, and with the appropriate boundary conditions.

One now proceeds as follows:

(i) Two Fourier transforms are performed, first along the x direction and then along the y direction.

(ii) The resulting one-dimensional problems along the z direction are solved using either the classical Gauss elimination method or a step-by-step method.

(iii) Reconstitution of the solution is done via two inverse Fourier transforms first along the y-direction and then along the x direction.

The operation count shows that if M and N are the number of mesh points, of the form $M = 2^{Q_M}$, $N = 2^{Q_N}$ along the x and y directions, and K along the z direction, the required number of operations for the complete solution of Eq. (75) is proportional to $MNK(\log_2 M + \log_2 N)$.

7.3. *Extension of the Method to Integro Differential Equations*

The only requirements for Eqs. (8) and (9) is that they must be symmetric in x—which is why one does not consider the $\partial\phi/\partial x$ term in Eq. (1)—and also that the corresponding computing molecule should be simple, i.e., expressible with at most three samplings in each direction.

The above constraints are satisfied if we add to the left-hand side of Eq. (1) a fifth term of the form:

$$\int\int \phi \, dx \, dy, \tag{76}$$

where the domain of integration is restricted to distances ΔX and ΔY in the neighborhood of a point and for which the finite difference counterpart for $\Delta X = \Delta Y$ is simply

$$\frac{(\Delta X)^2}{9} \times \begin{array}{ccc} 1 & 4 & 1 \\ 4 & 16 & 4 \\ 1 & 4 & 1 \end{array} \phi(*, *). \tag{77}$$

7.4. *Inclusion of a First-Derivative Term with Respect to x*

If one adds to the left-hand side of Eq. (1) a fifth term of the form $\lambda(\partial\phi/\partial x)$, stencil equations (15) and (16) become, respectively,

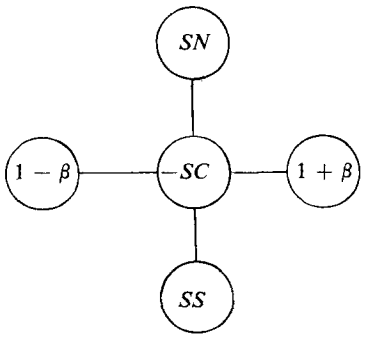

$$\phi(*, *) = \Gamma(I, J) \tag{78}$$

and

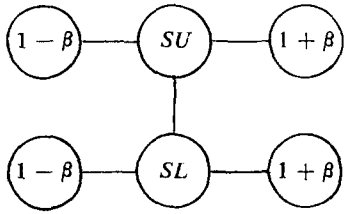

$$\phi(*, *) = \qquad \Gamma(*, *), \tag{79}$$

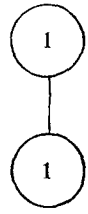

where $\beta = (\lambda/2)\,\Delta X$ and ΔX is chosen such that $\beta < 1$.

In this case, the only change for x-condition 3(a) is the replacement of $U(I, J)$ by $U(I, J)\,\alpha^I$ where $\alpha = \sqrt{(1 + \beta/1 - \beta)}$ and one has

Analysis

$$U_S(J) = \frac{2}{M} \sum_{I=1}^{M-1} U(I, J)\,\alpha^I \sin\left(\frac{\pi SI}{M}\right) \qquad (1 \leqslant S \leqslant M - 1); \tag{80}$$

Synthesis

$$U(I, J) = \alpha^{-I} \sum_{S=1}^{M-1} U_S(J) \sin\left(\frac{\pi IS}{M}\right) \qquad (1 \leqslant I \leqslant M - 1). \tag{81}$$

Also, system (18) is modified accordingly ,

$$\begin{aligned} \Gamma(1, J) &:= \Gamma(1, J) - (1 - \beta)\,\phi_L(J), \\ \Gamma(M - 1, J) &:= \Gamma(M - 1, J) - (1 + \beta)\,\phi_R(J), \end{aligned} \tag{82}$$

while in Eqs. (36), (37) $\cos(\pi S/M)$ is multiplied by $\sqrt{(1 - \beta^2)}$. A similar result has been obtained somewhat differently by Sarmin [7].

7.5. *Concluding Remarks*

The present fast Fourier transforms have been successfully used for the two-dimensional solution of both the Laplace and the Poisson equations. In cylindrical geometry with azimuthal symmetry, the above techniques were applied in plasma simulation [8], while the planar version of Poisson's equation has been used in the simulation of high-intensity proton-beam accelerators [9]. The foregoing numerical studies made ample use of techniques described by Hockney [1] for the specification of either inside boundaries or free-space conditions. The general two-dimensional code for the solution of Eq. (1) should also find application in nuclear-reactor calculations [10] where one has to solve several adjacent rectangular regions each with their own set of coefficients for the partial differential equation; in this case

the FFT techniques would be used in each subdomain, and the treatment of interfaces between the different material regions could be performed iteratively.

Three-dimensional problems have also been solved. The first one, which arose with magnetic field evaluation for high-energy physics magnets [11], solves the Laplace equation on a $64 \times 64 \times 10$ mesh (that is, 40960 cells) in 8.4 sec on the CERN CDC 6600 computer with a relative precision of 10^{-11}. The second one sprang from the study of magnetic field penetration into a two-dimensional iron block, and led to a three-dimensional parabolic equation (the time being thought of as a dimension) which, due to the evolutive character of the problem, was solved in "slices" of eight cells in the time direction for memory requirements. Altogether, a $64 \times 64 \times 80$ mesh (roughly a third of a million cells) required 80 sec on the CERN CDC 6600 computer, and was checked against an analytical study [12] for very simple boundary conditions. A general three-dimensional computer code for the solution of Eq. (75) will be developed in the near future. However, the limited direct access memory of the largest present-day computers causes a bottleneck, and much is hoped in that direction from new machines such as the Illiac IV and Star 100 computers.

Acknowledgments

The author wishes to express his gratitude to the Institute for Plasma Research, Stanford University, where this work was initiated, and to the Synchrotron Injector Division of CERN for the financial support during the period when the computational codes were developed. He would also like to acknowledge the rewarding discussions with Professors O. Buneman and G. Golub at Stanford and Professor P. Lapostolle at CERN, and to express his thanks to Dr. Ch. Iselin of CERN for programming an optimized FFT code and to Mr. D. Lamotte who provided the program for the graphical display. The author is also very grateful to the CERN Scientific Typing Service for the accurate typing of this report.

References

1. R. W. Hockney, The potential calculation and some applications, *in* "Methods in Computational Physics," Vol. 9, Academic Press, Inc., New York and London, 1969.
2. O. Buneman, SUIPR Report No. 294, Institute for Plasma Research, Stanford University, May 1969.
3. R. Le Bail, SUIPR Report No. 314, Institute for Plasma Research, Stanford University; also, Internal report CERN/SI/Int. Rep. DL/70-11 (1970).
4. B. Buzbee, G. Golub, and C. Nielson, Reports CS-128 and CS-155, Computer Science Dept., Stanford University, 1969.
5. L. Collatz, "The numerical treatment of differential equations," pp. 542, 543, Springer-Verlag, New York, 1966.
6. C. Lanczos, "Linear differential operators," pp. 456–464, D. Van Nostrand Company, Inc., London, 1961.

7. E. N. SARMIN, Application of the method of straight lines to the solution of boundary value problems for certain non-conjugate two-dimensional second-order elliptic equations, *U.S.S.R. Comput. Math. and Math. Phys.* **5**, No. 5 (1965), 240–246.
8. R. LE BAIL, Plasma computer simulation in cylindrical geometry with azimuthal symmetry, Doctoral thesis, Stanford University, California, June, 1970.
9. P. LAPOSTOLLE, Possible emittance increase through filamentation due to space charge in continuous beams, Particle Accelerator Conference, Chicago, 1971.
10. W. C. SANGREN, "Digital computers and nuclear reactor calculations," pp. 80–90, John Wiley and Sons, Inc., New York, 1960.
11. H. WIND, Evaluating magnetic field component from boundary observations only, *Nucl. Instrum. Methods* **84** (1970), 117–124.
12. G. BRIANTI, I. GUMOWSKI, AND K. SCHINDL, Behaviour of the magnetic induction B in solid steel coves submitted to an excitation variable with time, Internal report CERN/SI/Int. DL/71-3 (1971).